422 *Biochemistry* **2010,** *49,* 422–431
DOI: 10.1021/bi901525m

BIOCHEMISTRY
including biophysical chemistry & molecular biology
Article

Na^+ and K^+ Allosterically Regulate Cooperative DNA Binding by the Human Progesterone Receptor[†]

Keith D. Connaghan, Aaron F. Heneghan, Michael T. Miura, and David L. Bain*

Department of Pharmaceutical Sciences, University of Colorado Denver, Aurora, Colorado 80045

Received August 31, 2009; Revised Manuscript Received November 17, 2009

ABSTRACT: Cooperativity is a common mechanism used by transcription factors to generate highly responsive yet stable gene regulation. For the two isoforms of human progesterone receptor (PR-A and PR-B), differences in cooperative DNA binding energetics may account for their differing transcriptional activation properties. Here we report on the molecular origins responsible for cooperativity, finding that it can be activated or repressed with Na^+ and K^+, respectively. We demonstrate that PR self-association and DNA-dependent cooperativity are linked to a monovalent cation binding event and that this binding is coupled to modulation of receptor structure. K^+ and Na^+ are therefore allosteric effectors of PR function. Noting that the apparent binding affinities of Na^+ and K^+ are comparable to their intracellular concentrations and that PR isoforms directly regulate the genes of a number of ion pumps and channels, these results suggest that Na^+ and K^+ may additionally function as physiological regulators of PR action.

Progesterone receptors (PR)[1] are members of the steroid receptor family of ligand-activated transcription factors (*1*). The traditional understanding of PR function is that ligand-bound receptors dimerize in solution, bind to progesterone response elements (PREs) located within PR-regulated promoters, and recruit an array of coactivating proteins in order to remodel chromatin and activate transcription. Although PR function is well understood within this biochemical framework, we have yet to achieve a more fundamental and quantitative understanding. Specifically lacking are the physical rules and molecular states associated with receptor assembly at complex promoter sequences and the chemical mechanisms by which these events are coupled to transcriptional activation. This lack of knowledge is in part due to the great complexity of receptor function, but it also arises because receptor activity has largely been studied using only qualitative and semiquantitative approaches, despite the fact that PR-mediated transcriptional activation is a fundamentally quantitative process.

Any understanding of PR function is further complicated by the fact that the receptor exists naturally as two distinct isoforms, PR-A and PR-B (*2*). As shown in Figure 1, the two isoforms are identical except for an additional 164 residues at the N-terminus of PR-B. Yet despite their near sequence identity, the two isoforms maintain numerous differences in function (*3*−*9*). In particular, PR-B is typically the stronger transcriptional activator and regulates the bulk of PR-regulated genes (*8*). And yet the smaller A-isoform, even when in the presence of equimolar concentrations of PR-B, is able to preferentially activate gene expression at remaining promoter sites. The mechanisms by which the two isoforms can maintain differences in transcriptional activity at any particular promoter and the principles they utilize to generate opposing results at other promoters are largely unknown. Our research is focused on the molecular origins of this behavior, using the results as a paradigm for understanding the receptor-specific activities for all of the proteins that define the steroid receptor family.

As a step toward integrating the physical and chemical properties of PR isoforms with their biological roles, we previously examined the thermodynamics of PR-A and PR-B interactions with complex promoter sequences (*10*−*12*). The results of this work revealed a number of unexpected findings, some of which were contrary to the biochemically based model of function. For example, despite the fact that both isoforms have identical DNA binding domains, the receptors maintain large differences in DNA binding energetics (*10*). Most notably, the B-isoform has greatly enhanced cooperative interactions when binding at multiple response elements relative to PR-A. Thus PR-B binding to a promoter containing two identical palindromic progesterone response elements (PRE_2) is accompanied by a −3 kcal/mol or ∼200-fold increase in stabilization, whereas PR-A binding is coupled to a more modest 5-fold increase. This large difference accurately predicts differential PR-A and PR-B promoter occupancy (and thus differential transcriptional activation) at physiological conditions and suggests that it is cooperativity rather than simply DNA binding that is the key determinant of isoform-specific function. Consistent with this hypothesis, later work demonstrated that the ability of the receptors to efficiently recruit coactivators is coupled more to the extent of cooperative interactions rather than to simply DNA binding (*13*). Thus cooperativity and transcriptional activation appear to be linked phenomena. Left unrevealed in these studies, however, were the molecular forces responsible for cooperative assembly.

For PR and nearly all other transcription factors, the mechanisms underlying cooperativity are poorly understood, even though cooperative interactions have been observed in gene regulatory systems ranging from bacteriophage to human (*10*, *14*−*18*). Here

[†]This work was supported by the Avon Foundation for Women and NIH Grant DK061933 to D.L.B.

*To whom correspondence should be addressed. Phone: (303) 724-6118. Fax: (303) 724-7266. E-mail: David.Bain@ucdenver.edu.

[1]Abbreviations: PR, progesterone receptor; PR-A, progesterone receptor A-isoform; PR-B, progesterone receptor B-isoform; M^+, monovalent cation; DBD, DNA binding domain; HBD, hormone binding domain; AF, activation function; BUS, B-unique sequence; H, hinge; PAGE, polyacrylamide gel electrophoresis; DTT, dithiothreitol.

 Published on Web 12/15/2009

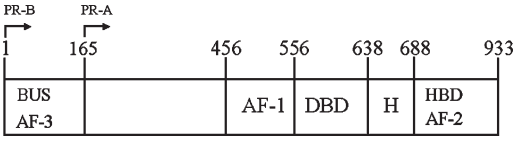

FIGURE 1: Schematic of PR isoform primary sequence. Functional regions are as indicated: HBD, hormone binding domain; DBD, DNA binding domain; H, hinge; AF, activation functions; BUS, B-unique sequence. PR-A is defined as amino acids 165−933.

we examine the chemical mechanism of cooperativity by investigating the role of ion type in controlling PR function. We demonstrate that monovalent cations (M^+) of the group 1a alkali earth metal series (Li^+, Na^+, K^+, Rb^+, and Cs^+) modulate the functional properties of both PR-A and PR-B. This occurs at the level of self-association in the absence of DNA and in the degree of cooperativity when bound to DNA. These ions are thus allosteric effectors that directly control PR function. Consistent with this, limited proteolysis studies reveal cation-specific regulation of PR structure. Finally, since the apparent binding affinity of the physiologically relevant cations Na^+ and K^+ are in the low millimolar range (therefore comparable to their intracellular concentrations) and PR isoforms regulate a number of genes encoding ion pumps and channels, we speculate that these ions may also play important roles as regulatory ligands *in vivo*.

MATERIALS AND METHODS

Expression, Purification, and Characterization of Full-Length, Human Progesterone Receptor Isoforms. Expression vectors encoding either human PR-A (residues 165− 933) or PR-B (residues 1−933) fused to an N-terminal hexahistidine tag were a gift from Dr. Dean Edwards (Baylor University). Each isoform was expressed in baculovirus-infected Sf9 insect cells using standard protocols (*19*). We previously characterized the thermodynamics and hydrodynamics of both PR isoforms in order to ensure that the purified proteins were amenable to rigorous analysis. Briefly summarized, each receptor was purified to at least 95% homogeneity and subjected to extensive sedimentation velocity and equilibrium analyses (*20*, *21*). These studies demonstrated that, in buffers containing only Na^+ as the monovalent cation, each isoform maintained exclusively a monomer−dimer equilibrium in the micromolar range ($\Delta G_{\text{dimerization}} = -7$ kcal/mol). Just as importantly, the results also demonstrated that both isoforms were structurally and functionally homogeneous. Finally, we note that our previous work on PR and PR deletion constructs indicates that the hexahistidine tag has no detectable influence on the properties of the protein (*22*, *23*) and that the tagged receptor maintains high functional activity (*10*−*13*, *20*, *21*).

Sedimentation Velocity and Equilibrium Analyses as a Function of Monovalent Cation Type. All sedimentation analyses were carried out on a Beckman XL-A analytical ultracentrifuge equipped with absorbance optics and an An-60 Ti rotor. For the velocity studies, the isoforms were loaded at an initial concentration of 1.0 μM and sedimented at 4 °C in MCl concentrations ranging from 10 to 300 mM. The remaining buffer contained 20 mM Tris, pH 8.0, 2.5 mM $MgCl_2$, 1 mM $CaCl_2$, 1 mM DTT, and 10^{-5} M progesterone. Tris rather than Hepes (as used in our previous studies) was used as a buffering agent in order to titrate all MCl solutions with HCl; this ensures that only one type of monovalent cation is present in solution. We have found no evidence that PR function is differentially influenced by Hepes and Tris, nor is there any evidence that PR thermodynamics are influenced by the Mg^{2+} or Ca^{2+} ions present in solution (necessary for carrying out the DNase footprinting studies).

Each isoform was sedimented at a rotor speed of 50000 rpm, with data collected at 230 nm and as quickly as the instrument would allow (typically every 4 min). A two-channel Epon centerpiece was used in all experiments. The sedimentation coefficient distribution, $g(s^*)$, and weight-average sedimentation coefficient, at each PR concentration were calculated as implemented in the program DCDT+ (*24*, *25*). Each distribution was corrected to 20 °C and water ($s_{20,w}$) using standard methods (*26*), where $s_{20,w}$ is defined as

$$s_{20,\,w} = \frac{M(1-\bar{\nu}\rho)}{Nf} \quad (1)$$

M is the weight-average molecular weight as determined by the amino acid sequence and assembly stoichiometry, $\bar{\nu}$ is the partial specific volume of the protein, ρ is the water density at 20 °C, and N is Avogadro's number. The partial specific volume for both isoforms was calculated by summing up the partial specific volumes of each individual amino acid (0.7302 mL/g) (*27*).

The sedimentation equilibrium studies were carried out in 50 mM KCl, using otherwise identical buffer and temperature conditions as described for the sedimentation velocity experiments. Samples were allowed to reach equilibrium using six-channel Epon centerpieces. Three PR-B concentrations were analyzed at a ratio of 4:2:1, with the highest loading concentration being 0.9 μM. Samples were equilibrated at 14000, 18000, and 21000 rpm and judged to be at equilibrium by successive subtraction of scans. The nine data sets (three concentrations collected at three rotor speeds) were analyzed individually and globally using the nonlinear least-squares (NLLS) parameter estimation as implemented in the program NONLIN (*28*).

Data were fit to the following equation in order to resolve the self-association equilibrium constants:

$$Y_r = \delta + \alpha \exp[\sigma(r^2 - r_0^2)] + \sum \alpha^n K_n \exp[n\sigma(r^2 - r_0^2)] \quad (2)$$

where Y_r is absorbance at radius r, δ is the baseline offset, and α is the monomer absorbance at the reference radius, r_0. σ is the reduced molecular weight (eq 3), n is the stoichiometry of the reaction, and K_n is the product association constant of the reaction $n\text{M} \leftrightarrow \text{M}_n$.

σ, the reduced molecular weight, is defined as

$$\sigma = \frac{M(1-\bar{\nu}\rho)\omega^2}{RT} \quad (3)$$

where M is the weight-average molecular weight of a single, ideal species, $\bar{\nu}$ is the partial specific volume of PR-B, ρ is the solvent density (as calculated on the basis of the salt composition and temperature (*29*)), ω is the angular velocity, R is the gas constant, and T is the temperature in kelvin. The σ for the global analysis was fixed at a value corresponding to the molecular weight (M) and partial specific volume ($\bar{\nu}$) of the PR-B monomer. Resolved values of K_n were converted from absorbance to molar association constants on the basis of the calculated ε_{230}. Free energies for the assembly reactions were calculated using $\Delta G_n = -RT \ln K_n$. In all experiments used for analysis, salt-dependent changes in pH were determined to be negligible, as were any salt-induced changes in water activity (*30*).

DNA Preparation for DNase I Footprinting. A vector containing a promoter made up of two tandemly linked PREs

(PRE_2) was a gift from Dr. Kathryn Horwitz (University of Colorado Denver). Each PRE corresponds to an imperfect palindrome within the tyrosine aminotransferase promoter, TGTACAGGATGTTCT (*31*) spaced 25 base pairs apart. A reduced-valency template (PRE_{1-}) containing a G-to-T point mutation in each half-site of the distal PRE (designated as site 1) was created "in house". Each template was excised from its respective vector to generate a 1304 bp promoter fragment and ^{32}P-end-labeled. The proximal PRE of each fragment (site 2) was positioned 100 bp from the 3′ end of the labeled strand.

Individual-Site Binding Experiments. Experiments were carried out using quantitative DNase I footprint titrations as originally described by Ackers and co-workers (*32*, *33*), with the following modifications. All reactions were carried out in an assay buffer containing either 50 mM KCl or NaCl and the following components: 20 mM Hepes, 1 mM DTT, 1 mM $CaCl_2$, 2.5 mM $MgCl_2$, 10^{-5} M progesterone, 100 μg/mL BSA, and 2 μg/mL salmon sperm DNA. (The addition of BSA and salmon sperm DNA changes the concentration of Na^+ or K^+ by less than 1%). Other than the type of monovalent cation, these conditions are identical to our earlier footprinting analyses (*10*−*13*). The respective buffers were titrated to pH 8.0 using either KOH or NaOH in order to maintain constant ion type. Six KCl footprint reactions were performed, three on the PRE_2 promoter and three on the PRE_{1-} promoter. Two NaCl footprint reactions were carried out, one on the PRE_2 promoter and one on the PRE_{1-} promoter.

Each footprinting reaction contained 20000 cpm of freshly labeled DNA containing either the PRE_2 promoter or PRE_{1-} promoter. PR-B was added to each reaction mix, covering a concentration range from subnanomolar to micromolar, and allowed to equilibrate at 4 °C for at least 45 min. DNase I (Invitrogen) was diluted to a concentration of 0.0058 unit/μL in the respective assay buffer less BSA and salmon sperm DNA. After the samples reached equilibrium, 5 μL of the diluted DNase I solution was added to each 200 μL reaction, and digestion was allowed to proceed for exactly 2 min. Digestion products were electrophoresed on 6% acrylamide−urea gels and visualized using phosphorimaging. Individual-site binding isotherms were calculated as described by Brenowitz et al. (*32*) using the program ImageQuant. All studies were carried out with DNase concentrations low enough to generate "single-hit kinetics" and therefore thermodynamically valid binding isotherms (*33*). Finally, promoter DNA concentrations were estimated to be well below PR-B binding affinity (maximally 5 pM), justifying the assumption that $PR\text{-}B_{free} \cong PR\text{-}B_{total}$.

Resolution of Microscopic Interaction Free Energies. The DNase I footprint titration technique resolves the fractional occupancy of binding at each PRE. The statistical thermodynamic expressions that describe the individual-site binding isotherms are constructed by summing the probabilities of each microscopic configuration that contributes to binding at each site. A detailed approach for generating each mathematical formulation has been presented previously (*15*). Briefly, the probability (f_s) of any microscopic configuration is defined as (*34*)

$$f_s = \frac{e^{(-\Delta G^\circ_s/RT)}[x_2]^j}{\sum_{s=1}^{j} e^{(-\Delta G^\circ_s/RT)}[x_2]^j} \quad (4)$$

where ΔG°_s is the free energy of configuration state s relative to the unliganded reference state, x_2 is the PR-B dimer concentration, j is the stoichiometry of the PR-B dimer bound to a response element, R is the gas constant, and T is temperature in kelvin. The dimer concentration is calculated using the experimentally determined dimerization constant (k_{di}) from the sedimentation equilibrium studies and the appropriate conservation of mass equation.

The fractional saturation ($\bar{Y}$) for dimer binding at any site on the PRE_2 promoter is the sum of probabilities for the isolated dimer binding event and the cooperative interaction with the adjacently bound dimer. Thus, the equation for PR-B dimer binding to site 1 on the PRE_2 promoter is defined as

$$\overline{Y}_{PRE_2} = \frac{kx_2 + k^2k_c{x_2}^2}{1 + 2kx_2 + k^2k_c{x_2}^2} \quad (5)$$

where x_2 is as defined previously, k is the intrinsic association constant for a preformed dimer binding to a PRE, and k_c corresponds to the intersite cooperativity term. Because the PREs are identical in sequence, eq 5 also describes binding to site 2 of the PRE_2 promoter. Using the same approach, the equation describing the fractional saturation of site 2 of the PRE_{1-} promoter is

$$\overline{Y}_{PRE_{1-}} = \frac{kx_2}{1 + kx_2} \quad (6)$$

In order to resolve the interaction parameters describing PR-B−DNA binding, the isotherms from each footprint titration were analyzed globally using the program Scientist (Micromath, Inc.). Because protein interactions at DNA binding sites do not afford complete protection from DNase activity, binding data were treated as transition curves fitted to upper (m) and lower (b) end points:

$$\overline{Y}_{app} = b + (m - b)\overline{Y} \quad (7)$$

Limited Proteolysis. Sequencing grade trypsin was obtained from Roche Applied Science (Indianapolis, IN). A 1 μM concentration of PR-B was digested in the identical buffer and temperature conditions as described for the sedimentation velocity studies using either 300 mM NaCl or 300 mM KCl. Enzyme was added at a PR:enzyme mass ratio of 500:1. Each reaction was allowed to proceed for 90 min with aliquots removed as a function of time. In order to ensure trypsin maintained a constant activity as a function of cation type, digests of control proteins were performed in NaCl and KCl buffers. These digests produced identical results, as predicted by the structural and biophysical work of Di Cera and co-workers (*35*). Reactions were terminated by addition of SDS−PAGE loading dye and boiling for 5 min. Five micrograms of PR was electrophoresed using 10% SDS−PAGE and transferred to nitrocellulose membrane for immunoblot analysis. The antibody used for analysis was C-19, a polyclonal antibody specific for the C-terminal portion of the PR hormone binding domain obtained from Santa Cruz Biotechnology (Santa Cruz, CA).

RESULTS

The traditional model for PR function is that receptors dimerize and then bind to their response elements; binding at multiple sites can potentially be coupled to cooperative interactions (*1*, *36*). This pathway is presented schematically in Figure 2. Also listed are the microscopic interaction constants for each of these reactions (k_{di}, k, k_c). Each of the terms defines a physically

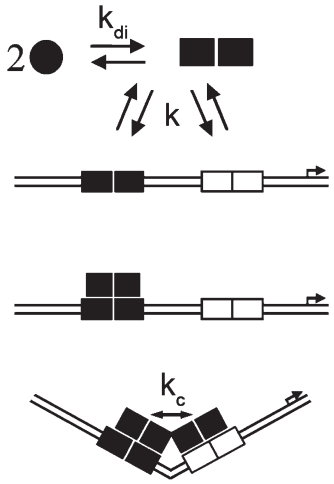

FIGURE 2: Schematic of selected assembly states for PR−PRE_2 interactions. Dimer binding pathway: Circles represent hormone-bound PR monomers. Squares represent PR solution dimers or PR bound to the PRE_2 promoter (k). Binding at multiple response elements is accompanied by an intersite cooperative interaction (k_c). Events potentially associated with cooperativity are indicated by protein−protein contacts and bending of promoter DNA. The arrow refers to the direction of the transcriptional start site.

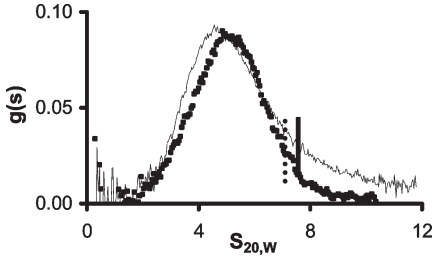

FIGURE 3: Sedimentation velocity analysis of PR-B in either NaCl or KCl. The initial loading concentration of PR-B for both NaCl (filled squares) and KCl (line) was 1.0 μM. $g(s^*)$ distributions were determined by analysis of successive scans taken in each salt. Vertical lines indicate the weight-average sedimentation coefficient determined by analysis of each $g(s^*)$ distribution in NaCl (dotted line) and KCl (solid line). In addition to either 50 mM NaCl or 50 mM KCl, buffer conditions were 20 mM Tris, pH 8.0, 2.5 mM $MgCl_2$, 1 mM $CaCl_2$, 1 mM DTT, and 10^{-5} M progesterone at 4 °C.

meaningful interaction event and should therefore be contrasted with the macroscopic, apparent binding affinities more commonly used in measuring receptor−DNA interactions. These latter parameters are at best a composite of multiple interactions and thus offer little mechanistic insight. Here we take the approach of determining each of the microscopic parameters as a function of Na^+ and K^+ as a means to delineate the chemical mechanism responsible for PR cooperative promoter binding. Sedimentation studies were used to examine the self-association properties of the PR isoforms (thus accounting for k_{di}), and quantitative footprint titrations were used to determine the intrinsic dimer DNA binding affinity (k) and intersite cooperativity (k_c).

Na^+ and K^+ Modulate the Self-Association of PR Isoforms. Our previous work on PR-B demonstrated that when in the presence of 50 mM NaCl the receptor undergoes rapid monomer−dimer exchange in the micromolar range (*21*). Sedimentation velocity was used to extend these studies by examining the influence of other monovalent cation types. As an example, plotted in Figure 3 are the $g(s)$ sedimentation coefficient distributions for 1.0 μM PR-B determined in a buffer containing 50 mM NaCl and in an equivalent concentration of KCl. Note that the weight-average sedimentation coefficient for PR-B ($s_{20,w}$, noted as vertical lines) increases from 7.1 s in Na^+ to 7.6 s in K^+ due to a rightward shift in the overall distribution. Identical results were seen for PR-A (data not shown). From the Svedberg equation (eq 1), an increase in $s_{20,w}$ can occur from either an increase in average molecular weight (M) due to increased self-association or a decrease in the frictional coefficient (f) due to compaction of macromolecular structure. As we will demonstrate below, the skewing of the distribution to larger $s_{20,w}$ values is due to formation of PR-B assembly states beyond that of the dimer.

Shown in Figure 4 are sedimentation equilibrium results for PR-B carried out in the identical KCl buffer as used in the velocity experiment. The three concentrations consist of PR-B loaded at a ratio of 4:2:1 with the highest concentration being 0.9 μM. Data from each concentration and rotor speed were first individually fit to resolve the average molecular weight of the sample; this analysis revealed a strong increase in apparent

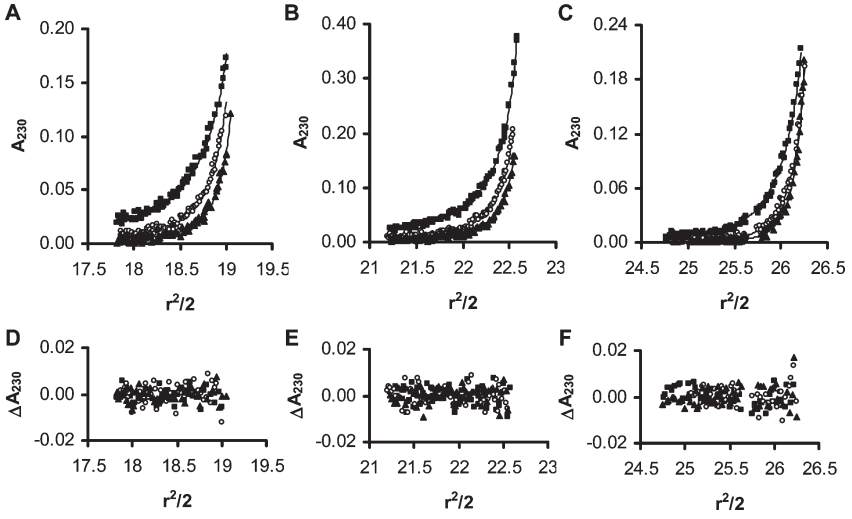

FIGURE 4: PR-B sedimentation equilibrium in 50 mM KCl. Panels A−C represent each initial loading concentration: 0.9 μM (panel A), 0.45 μM (panel B), and 0.25 μM (panel C). Symbols represent PR-B absorbance at 14000 rpm (filled squares), 18000 rpm (open circles), and 21000 rpm (filled triangles). Solid lines represent the best fit model (monomer−dimer−pentamer) from simultaneous analysis of all nine data sets. The square root of the variance was 0.004 absorbance units. Panels D−F show residuals from the monomer−dimer−pentamer equilibrium model plotted as a change in absorbance versus radius squared divided by 2. For the sake of clarity only every other residual point is plotted. Buffer conditions were 20 mM Tris, pH 8.0, 50 mM KCl, 2.5 mM $MgCl_2$, 1 mM $CaCl_2$, 1 mM DTT, and 10^{-5} M progesterone at 4 °C.

Table 1: Resolved Self-Association Energetics of PR-B in either KCl or NaCl

interaction free energy	KCl (kcal·mol^{-1})	NaCl (kcal·mol^{-1})	$\Delta\Delta G$ (kcal·mol^{-1})
ΔG_{di}	-7.6 ± 0.3	-7.2 ± 0.7	-0.4 ± 0.8
ΔG_{pent}	-30.9 ± 0.3		

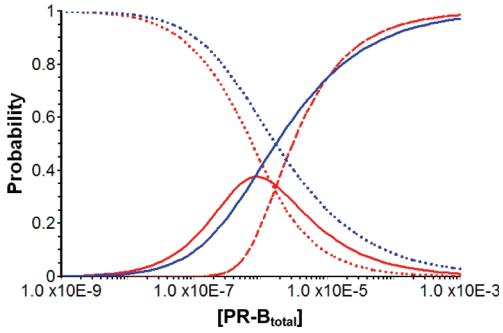

FIGURE 5: Calculated probabilities for PR-B solution assembly states in 50 mM NaCl or KCl. Shown are the probabilities for PR-B monomers (dotted line), dimers (solid line), and pentamers (dashed line) in solutions containing either 50 mM NaCl (blue) or 50 mM KCl (red).

molecular weight as receptor concentration was increased, as would be predicted for a self-associating system. The data were then globally fit to various assembly schemes (e.g., monomer−dimer, momomer−trimer) noting the quality of each fit. The data were best described by an equilibrium distribution of PR-B monomers, dimers, and pentamers (solid lines through data), although models incorporating either tetramers or hexamers were also consistent with the data. By contrast, attempts to force a fit using the traditional monomer−dimer association scheme returned an unacceptable result, as judged both by visual inspection and by a significantly increased standard deviation of the fit (data not shown). Consequently, it can be concluded that the assembly in K^+ is significantly increased compared to Na^+; however, a determination of the number of higher order assembly states and their exact stoichiometries is not possible.

Shown in Table 1 are the resolved assembly energetics and a comparison to our previous sedimentation equilibrium studies on PR-B in 50 mM NaCl (*21*). It can be seen that changing the monovalent ion type from Na^+ to K^+ has no statistically significant effect on the dimerization energetics. The more striking difference is that K^+ induces the formation of higher order species not seen with Na^+. As noted, these species were best described assuming the formation of PR-B pentamers but could also be fit as tetramers or hexamers. This is because, at 50 mM KCl, there is only a small proportion (maximally 10% of the total population) of these higher order species, making an exact characterization of the distribution difficult. As such, it is also difficult to determine if the larger species are reversibly associating or are a nonreversible aggregate. As we will subsequently show using the remaining group 1a salts, these higher order assembly states represent an "aporeceptor" population not bound by K^+. The calculated species distribution for the various assembly states is plotted as a function of total PR concentration in Figure 5.

N^+ and K^+ Modulate Cooperative Binding Energetics. We next assessed the role of Na^+ and K^+ in PR function by dissecting the energetics of binding to a promoter containing two identical response elements (PRE_2; see Figure 2). As a first step in this assessment, footprint titrations were carried out in a KCl buffer identical to that used in the sedimentation velocity and equilibrium studies. Shown in Figure 6A is a representative PR-B footprint titration of the PRE_2 promoter in said buffer. Binding isotherms for sites 1 and 2 are shown in Figure 6B. Also shown are isotherms generated from a mutated promoter containing only one competent response element (PRE_{1-}).

The footprint titrations were then repeated under identical conditions except that KCl was replaced with NaCl. The resultant isotherms are shown in Figure 6C. Visual comparison of the K^+ and Na^+ data sets makes clear that the apparent binding affinity of PR-B is decreased in KCl relative to NaCl. In particular, there appears to be little cooperative binding in KCl as evidenced by the near-identical binding isotherms seen for the PRE_2 and PRE_{1-} promoters. By contrast, the strong cooperativity in NaCl is observed in the leftward shift and increased steepness of the PRE_2 binding isotherms relative to the PRE_{1-} isotherm.

The three isotherms from each MCl data set were globally fit to eqs 5 and 6. The microscopic free energy changes (ΔG_i) for receptor−promoter binding in each salt are shown in Table 2, as are the differences in the energetics ($\Delta\Delta G_i$). It is evident that there is only a slight effect in the cation-dependent binding energetics of the PR-B dimer, with the affinity weakening only 0.9 kcal/mol when Na^+ is replaced with K^+. By contrast, there is an enormous change in the cooperativity term, with it decreasing 3.2 kcal/mol in the presence of K^+, thus entirely eliminating any cooperative interaction. These differences are not an artifact of cation-dependent changes in the active dimer concentration, since we explicitly accounted for this change using the resolved dimerization and pentamerization constants determined in each salt and the appropriate conservation of mass equations. Rather, these are true differences in PR-B binding and reveal that the primary consequence of changing monovalent cation type is not at the level of DNA binding *per se* but at the level of cooperative interactions between binding sites. With regard to the smaller A-isoform, a complete linkage analysis was not possible due to solubility issues in 50 mM KCl. However, we were unable to qualitatively detect any effect of KCl on PR-A assembly at the PRE_2 promoter. This result is as predicted since the cooperativity term in NaCl is already negligible and intrinsic binding energetics are not influenced by M^+ type.

PR Isoforms Bind a Monovalent Cation. The simplest explanation for the cation dependence to the sedimentation and footprinting data is that PR-B function is allosterically regulated by Na^+ and K^+ binding events. In order to more directly test this hypothesis, we carried out sedimentation velocity studies as a function of the chloride salts of the group 1a cations (LiCl, NaCl, KCl, RbCl, and CsCl). Plotted in Figure 7 are the resolved weight-average sedimentation coefficients for PR-B determined in these salts and at three salt concentrations. In 50 mM MCl, the sedimentation coefficient reaches a minimum when the protein is in Na^+ but reaches maximal values when determined in the cations at the extremes of the series (Li^+ and Cs^+). When the MCl concentration is decreased to 10 mM, the sedimentation coefficient increases only slightly in Na^+ but increases significantly in the presence of Li^+, K^+, and Rb^+. It is not clear how these ion-specific changes in PR-B sedimentation could be explained by simple electrostatic screening.

As was determined from our sedimentation equilibrium studies, the ion-specific increases in $s_{20,w}$ are due to the formation of

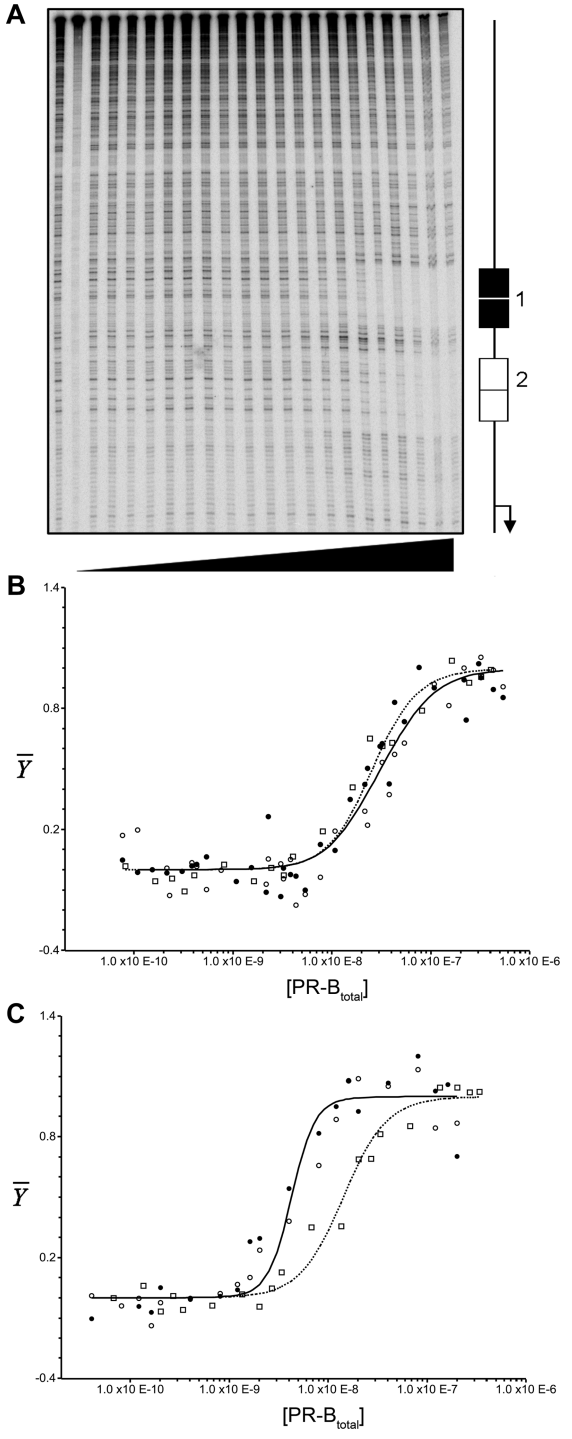

FIGURE 6: Representative quantitative footprint titration of PR-B binding to the PRE_2 promoter in KCl and individual site binding curves obtained for PR-B binding to both the PRE_2 and PRE_{1-} promoters in KCl and NaCl. Panel A: Representative footprint image of PR-B binding to the PRE_2 promoter in 50 mM KCl. Positions of the two PREs (site 1, filled rectangle; site 2, open rectangle) are indicated in the schematic to the right of the image. Panel B: All individual site binding isotherms for PR-B binding to site 1 (filled circles) and 2 (open circles) of the PRE_2 promoter and site 1 (open rectangle) of the PRE_{1-} promoter in 50 mM KCl. Also shown are the best fit lines from the model presented in Figure 2 describing binding to the PRE_2 (solid line) and PRE_{1-} (dotted line) promoters. The standard deviation of the fit was 0.074 apparent fractional saturation units. Panel C: All individual site binding isotherms from matched experiments for PR-B binding to the PRE_2 and PRE_{1-} promoters in 50 mM NaCl. Symbols and lines are as indicated in panel B. The standard deviation of the fit was 0.080 apparent fractional saturation units.

Table 2: Resolved Energetics and Differences for PR-B−PRE_2 Binding Interactions in KCl and NaCl

interaction free energy	KCl (kcal·mol^{-1})	NaCl (kcal·mol^{-1})	$\Delta\Delta G$ (kcal·mol^{-1})
ΔG	-11.7 ± 0.1	-12.6 ± 0.2	0.9 ± 0.2
ΔG_c	0.4 ± 0.4	-2.8 ± 0.1	3.2 ± 0.4

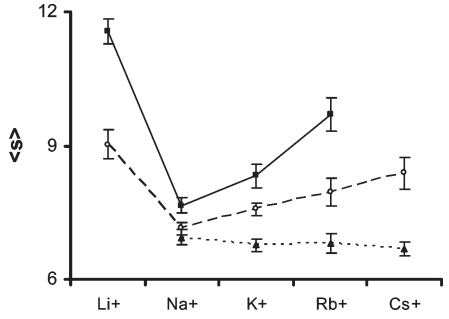

FIGURE 7: Measured PR-B weight-average s plot as a function of ion type and ion concentration. The initial PR-B loading concentration was 1.0 μM. The weight-average sedimentation coefficient was determined as implemented in the program DCDT+. Error estimates represent one standard deviation as reported by DCDT+. Solution conditions minus MCl were 20 mM Tris, pH 8.0, 2.5 mM $MgCl_2$, 1 mM $CaCl_2$, 1 mM DTT, and 10^{-5} M progesterone at 4 °C. The concentration of MCl was either 10 mM (squares, solid line), 50 mM (open circles, dashed line), or 300 mM (triangles, dotted line). M^+ is as indicated on the plot.

higher order species. This phenomenon is enhanced as the cations become larger in effective volume relative to Na^+. For example, the sedimentation coefficient in 10 mM Cs^+ was impossible to determine due to aggregation that caused complete precipitation of the receptor. With respect to a putative ion binding event, we interpret these results to mean that bulky cations like Cs^+ or highly hydrated ions like Li^+ are too large to interact at a M^+ binding site, resulting in enhanced assembly of that receptor fraction unable to bind cation (i.e., aporeceptors). By this logic, if the MCl concentration is made greater than the binding affinity of each cation, the sedimentation coefficient in all salts should reach a common value reflective of only PR-B monomers and dimers. As seen in Figure 7, the MCl concentration needed to saturate appears to be ~300 mM.[2]

Our observations are not unique to PR-B; as shown in Figure 8, a similar phenomenon is seen for PR-A. Again, a minimum in $s_{20,w}$ is found at Na^+ concentrations of 200 mM, with larger values seen at the extreme of the MCl series. The same qualitative result is seen at 100 mM NaCl and KCl, but again, data collected in 100 mM LiCl, RbCl, and CsCl were unanalyzable due to heavy precipitation. By contrast, when the MCl concentration is increased to 300 mM, Na^+, K^+, and Rb^+ generate the same value, suggesting that the receptor is saturated by the respective cations. It is worth noting that for both isoforms the increases in sedimentation coefficient seen at the extremes of the MCl series actually underestimate the extent of this phenomenon since we could not take into account larger assembly states that were quickly sedimented to the base of the solution

[2]We were unable to measure PR-B sedimentation behavior in 300 mM LiCl because at this concentration the salt generated a large change in pH. Correcting this change would have required acid or base addition sufficient enough to significantly perturb the total ionic strength.

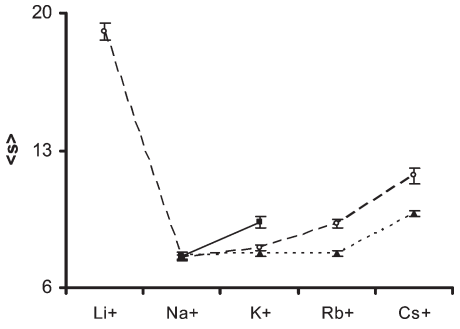

FIGURE 8: Measured PR-A weight-average *s* plot as a function of ion type and ion concentration. The initial PR-A loading concentration was 1.0 μM. The weight-average sedimentation coefficient was determined as implemented in the program DCDT+. Error estimates represent one standard deviation as reported by DCDT+. Solution conditions minus MCl were 20 mM Tris, pH 8.0, 2.5 mM $MgCl_2$, 1 mM $CaCl_2$, 1 mM DTT, and 10^{-5} M progesterone at 4 °C. The concentration of MCl was either 100 mM (squares, solid line), 200 mM (open circles, dashed line), or 300 mM (triangles, dotted line). M^+ is as indicated on the plot.

Table 3: Calculated Weight-Average Sedimentation Coefficients for PR-B and PR-A at Each MCl Concentration[a]

	PR-B ⟨s⟩		
M^+	300 mM MCl	50 mM MCl	10 mM MCl
Li^+		9.0 ± 0.3	11.6 ± 0.3
Na^+	6.9 ± 0.2	7.1 ± 0.1	7.7 ± 0.2
K^+	6.8 ± 0.1	7.6 ± 0.1	8.3 ± 0.2
Rb^+	6.8 ± 0.2	8.0 ± 0.3	9.7 ± 0.4
Cs^+	6.7 ± 0.1	8.4 ± 0.4	
	PR-A ⟨s⟩		
M^+	300 mM MCl	200 mM MCl	100 mM MCl
Li^+	11.2 ± 0.3	19.0 ± 0.4	
Na^+	7.6 ± 0.1	7.5 ± 0.2	7.6 ± 0.2
K^+	7.7 ± 0.2	8.0 ± 0.2	9.3 ± 0.3
Rb^+	7.7 ± 0.2	9.3 ± 0.2	
Cs^+	9.8 ± 0.2	11.7 ± 0.4	

[a]The weight-average sedimentation coefficient (⟨*s*⟩) was determined as implemented in the program DCDT+. Error estimates (±) represent one standard deviation as reported by DCDT+. Solution conditions minus MCl were 20 mM Tris, pH 8.0, 2.5 mM $MgCl_2$, 1 mM $CaCl_2$, 1 mM DTT, and 10^{-5} M progesterone at 4 °C.

column. The resolved sedimentation coefficients for both isoforms under each salt condition are presented in Table 3.

Na^+ and K^+ Modulate Receptor Structure. The sedimentation and footprinting data provide strong hydrodynamic and thermodynamic evidence that PR function is allosterically regulated by M^+ binding. From a structural perspective, allosteric ligands are typically capable of triggering conformational changes within their target macromolecule. We examined this possibility by carrying out limited proteolysis studies of PR-B as a function of NaCl and KCl. Shown in Figure 9 are time-course digests of PR-B using trypsin. These studies were carried out at 300 mM concentrations of KCl and NaCl in order to ensure that the receptors were saturated with their respective cations.

Comparison of the two digests indicates that Na^+ binding results in PR-B adopting a more enzyme-accessible conformation relative to K^+ binding, as evidenced by increased proteolysis of the full-length receptor. However, this result is not due to a global destabilization of the protein but occurs primarily because of the more rapid appearance of several fragments encompassed by bands 1 and 2 (with band 1 being indicative of the primary cleavage site). All of these fragments are reactive to a C-terminal anti-HBD antibody and have molecular masses ranging from 52 to 76 kDa (i.e., much greater than that of the isolated HBD; see Figure 1); therefore, the tryptic cleavage sites must be located with the N-terminal region of PR-B. Because the most prominent of these fragments (band 1) has a molecular mass less than that of even the smaller PR-A isoform, the cleavage site that generates this fragment must be in a region common to both isoforms. Likewise, the smallest of the fragments (band 2) roughly corresponds to a peptide containing at least AF-1, DBD, and HBD. Thus, the results indicate that the conformation of an N-terminal sequence common to both PR-A and PR-B is differentially modulated by Na^+ versus K^+ binding. Consistent with this, a similar proteolysis result was seen for PR-A (data not shown). Finally, increased digestion times produce a 31 kDa fragment that corresponds to the isolated HBD (band 3). This fragment appears to be generated at an enhanced rate in Na^+, but since it is likely a product from the fragmented receptor rather than the intact holoprotein, its relevance is unclear.

DISCUSSION

The results presented here are consistent with a specific M^+ binding event that is allosterically coupled to PR cooperativity. We first address the evidence in favor of M^+ binding. The sedimentation velocity and equilibrium studies are not easily explained by nonspecific Debye−Hückel screening since PR-A and PR-B self-association is clearly modulated in a cation-specific manner. The results are also inconsistent with a Hofmeister effect via "salting in" of the receptor since that would predict a rank order ability of $Cs^+ > Rb^+ > K^+ > Na^+ > Li^+$ rather than the observed result of $Na^+ > K^+ > Rb^+ > Cs^+ > Li^+$. Nor can the results be interpreted as arising from cation-specific changes in water activity since at these low to moderate MCl concentrations the changes are minor (less than 1% (*30*)) and largely identical for each ion.

We therefore postulate the following: (1) In the NaCl concentrations used in our sedimentation studies (Figures 7 and 8 and refs (*20*) and (*21*)), PR-B is fully saturated by a bound sodium ion(s) and thus exists only as monomers and dimers, and that cation binding affinity is equivalent in the monomer and dimer states of PR. (2) A decrease in the M^+ concentration below the ion binding affinity populates an aporeceptor not bound by ion. (3) Formation of the apoprotein leads to higher order self-association. This self-association is observed as an increase in the sedimentation coefficient in the velocity studies and tetramer−pentamer−hexamer formation in the KCl equilibrium studies. Consistent with this hypothesis, different monovalent anions (Br^-, I^-, etc.) show only muted differences at the concentrations used in the cation studies (data not shown).

With regard to M^+ regulated allostery, we observe that with only modest concentrations of Na^+ or K^+ the functional property of cooperativity can be selectively activated or repressed without greatly influencing intrinsic binding energetics. This is not occurring via some unknown functional attribute of the aporeceptor population, since footprinting studies in RbCl (data not shown) revealed a dramatic decrease in apparent DNA binding affinity as evidenced by a rightward shift in the binding curve. This decrease was well correlated with the increased production

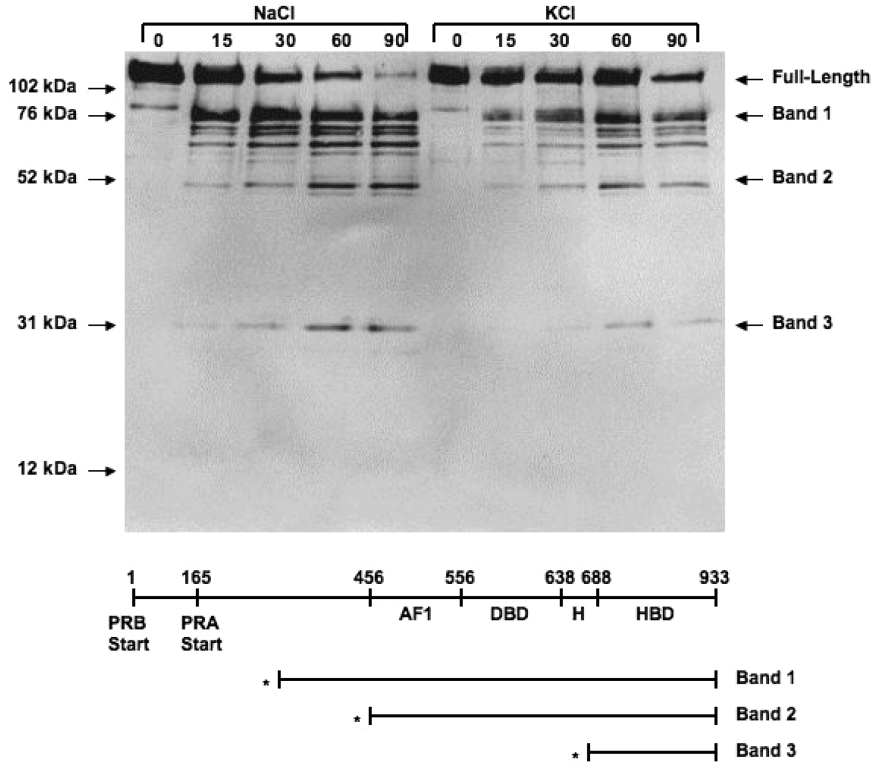

FIGURE 9: Time course for trypsin digestion of PR-B in NaCl vs KCl and mapped proteolytic fragments. One micromolar PR-B was digested using trypsin at 500:1 protein to enzyme mass ratio. Reactions were carried out at 4 °C in 20 mM Tris, pH 8.0, 2.5 mM $MgCl_2$, 1 mM $CaCl_2$, 1 mM DTT, 10^{-5} M progesterone, and 300 mM MCl. Reactions were allowed to proceed for 90 min with samples taken as a function of time. Resultant peptides were probed using immunoblot analysis and detected using anti-HBD antibody. *, fragment lengths are estimated using immunoblot analysis and apparent molecular mass.

of the higher order assembly states observed in the sedimentation velocity studies, suggesting that the aporeceptors are inactive with respect to promoter binding. Furthermore, the presence of each cation under saturating binding conditions (where only monomers and dimers are present) results in cation-specific changes in receptor structure. We thus conclude that Na^+ and K^+ are allosteric ligands that modulate the functional properties of the PR dimer. In this light, tetramers formed upon cooperative promoter binding and any potential tetramers made up of aporeceptors are distinct species as a result of Na^+'s unique ability to drive cooperativity. The exact structural basis for this difference is unknown.

The extent of M^+ binding should be dictated by two factors: the anhydrous radius of the ion and the size and strength of the hydration shell. For example, the small Li^+ ion (unhydrated atomic radius = 80 pm) maintains a strong charge density and thus generates a highly stable and large hydration shell (hydrated radius of 600 pm). Noting our sedimentation velocity data in LiCl (Figures 7 and 8), this hydrated volume must be too immense to easily fit within the putative ion binding pocket(s), thus resulting in a significant population of aporeceptor. A similar result is seen for Rb^+ and Cs^+ but by a different mechanism: These are large ions (unhydrated atomic radii of 180 and 210 pm, respectively) but generate weak hydration shells due to their decreased charge density. Nonetheless, like Li^+, they only weakly interact at the ion binding site, in this case because of their large anhydrous volumes. Since Na^+ and K^+ are of intermediate size (unhydrated atomic radii of 100 and 160 pm, respectively) and have moderate desolvation energetics, they can interact strongly with the receptor, with a slight energetic preference favoring Na^+. As predicted by this interpretation, any large bulky monovalent ion should also generate an increase in the sedimentation coefficient, and indeed, 200 mM ammonium chloride and choline chloride concentrations also generate $s_{20,w}$ values comparable to that of CsCl at the same concentration (data not shown).

If monovalent cations such as Na^+ and K^+ bind PR, they should have an affinity, a specific binding site, and a stoichiometry of binding. With regard to affinity, the sedimentation coefficients determined at each MCl concentration can be used as a rough guide. For example, in 300 mM CsCl the sedimentation coefficients for PR-A and PR-B are still highly elevated compared to that in NaCl, indicating that the binding affinity for Cs^+ must be in the very high millimolar range or greater. Following this logic, Rb^+ binding affinity must be only slightly below 300 mM, since for both isoforms the sedimentation coefficient in that salt is identical to that in NaCl, and yet the $s_{20,w}$ in RbCl increases significantly once the salt concentration drops even to 200 mM.

Focusing on the biologically relevant K^+ ion, at 300 mM KCl the sedimentation coefficient maintains the same value for both isoforms and in multiple salts. These data indicate that the binding site must be saturated, thus setting an upper limit for K^+ binding affinity of 300 mM. However, the sedimentation coefficient for both isoforms is statistically increased at 50 mM KCl. From fundamental binding theory this suggests that K^+ binding affinity is in the 10−100 mM range. Following a similar argument for Na^+, the $s_{20,w}$ for both PR-A and PR-B in NaCl is unperturbed from 50 to 300 mM, indicating that Na^+ binding affinity is at least below 50 mM. Specifically for PR-B, however, we observe an increase in $s_{20,w}$ when the salt concentration is decreased to 10 mM NaCl, indicating that Na^+ binding affinity is in the tens of millimolar range or less. Consistent with this,

footprinting studies using equimolar concentrations of 25 mM NaCl and KCl generated an intermediate ΔG_c term of -1.2 ± 0.2 kcal/mol, again suggesting that Na^+ binding affinity is in the low millimolar range. Nonetheless, these affinities can only be taken as approximate. We are currently attempting to measure Na^+ binding affinity more precisely by carrying out footprint studies over a range of Na^+ concentrations.

With regard to location of the binding site, both PR-A and PR-B follow similar trends in the sedimentation data; therefore, the location of the binding site(s) must be common to both isoforms. The structurally stable DBD or HBD might normally be attractive candidates; however, calculations using the program WASP (*37*) and the crystal structure coordinates of all available PR domains failed to identify any putative binding sites. This leaves only the N-terminal region common to both isoforms. As seen in Figure 9, this last possibility is supported by the limited proteolysis studies. Presumably, the structure of the N-terminal region is perturbed due to a proximal M^+ binding site. However, comparison of the PR sequence to the cation binding sequences of M^+ activated enzymes and monovalent cation channels showed no sequence homology. Unfortunately, the stoichiometry of binding cannot be addressed by the current data.

A millimolar M^+ binding affinity may seem surprisingly weak when compared to the micromolar or nanomolar affinities associated with PR dimerization and DNA binding (*10*−*12*, *20*, *21*). However, this affinity is comparable to intracellular M^+ concentration. Typical estimates place Na^+ concentration at 11−44 mM (see ref *38* and references cited therein) and K^+ concentration at 100−140 mM (*39*). This has at least two functional implications. First, a longstanding question in PR biology relates to how the two isoforms maintain their unique transcriptional regulation properties. In particular, if PR-B has a much greater binding affinity to a multisite promoter relative to PR-A (*10*), then the latter isoform should always be outcompeted for function. Our earlier computer simulations demonstrated, however, that if PR-B cooperativity was eliminated or PR-A cooperativity was increased when binding to a promoter sequence, then the smaller A-isoform could significantly increase its occupancy despite the fact that it has weaker intrinsic DNA binding energetics (*10*). These and our previous results (*11*) provide direct experimental support for this hypothesis; any minor decrease in Na^+ concentration or slight increase of K^+ concentration within the cell should significantly and preferentially decrease PR-B cooperative interactions with little influence on PR-A (since PR-A cooperative interactions are already minimal on promoters with architecture such as PRE_2).

Of additional biological relevance, PR isoforms are known to regulate a number of genes encoding various ion pumps and channels (*8*). In particular, the Na^+,K^+-ATPase β1 gene is directly and strongly regulated by PR-B. The promoter for this gene has been experimentally dissected and shown to contain multiple response elements capable of interacting with members of the steroid receptor family including the glucocorticoid receptor (*40*) and PR (Connaghan and Bain, unpublished data). We suspect that multiple response elements exist within PR-regulated promoters to thermodynamically link cooperativity with coactivator recruitment (*13*). In conjunction with the present results, this suggests that PR isoforms may act as ion sensors capable of controlling Na^+,K^+-ATPase β1 gene expression via a self-regulated feedback loop; any aberrant changes in Na^+ concentration will be allosterically coupled to changes in cooperative stabilization and thus coactivator recruitment, allowing PR-B to precisely control ATPase gene activity. Consistent with this, a number of studies have demonstrated that increased intracellular Na^+ levels trigger an increase in Na^+,K^+-ATPase β1 mRNA expression and protein production (*41*−*45*). We speculate then that Na^+ serves as a direct physiologic regulator of PR action. Cellular studies are currently underway in order to test this hypothesis.

ACKNOWLEDGMENT

We thank Dr. N. Karl Maluf for insightful discussions.

REFERENCES

1. Tsai, M. J., and O'Malley, B. W. (1994) Molecular mechanisms of action of steroid/thyroid receptor superfamily members. *Annu. Rev. Biochem. 63*, 451–486.
2. Kastner, P., Krust, A., Turcotte, B., Stropp, U., Tora, L., Gronemeyer, H., and Chambon, P. (1990) Two distinct estrogen-regulated promoters generate transcripts encoding the two functionally different human progesterone receptor forms A and B. *EMBO J. 9*, 1603–1614.
3. Meyer, M. E., Quirin-Stricker, C., Lerouge, T., Bocquel, M. T., and Gronemeyer, H. (1992) A limiting factor mediates the differential activation of promoters by the human progesterone receptor isoforms. *J. Biol. Chem. 267*, 10882–10887.
4. Sartorius, C. A., Melville, M. Y., Hovland, A. R., Tung, L., Takimoto, G. S., and Horwitz, K. B. (1994) A third transactivation function (AF3) of human progesterone receptors located in the unique N-terminal segment of the B-isoform. *Mol. Endocrinol. 8*, 1347–1360.
5. Meyer, M. E., Pornon, A., Ji, J. W., Bocquel, M. T., Chambon, P., and Gronemeyer, H. (1990) Agonistic and antagonistic activities of RU486 on the functions of the human progesterone receptor. *EMBO J. 9*, 3923–3932.
6. Mulac-Jericevic, B., Mullinax, R. A., DeMayo, F. J., Lydon, J. P., and Conneely, O. M. (2000) Subgroup of reproductive functions of progesterone mediated by progesterone receptor-B isoform. *Science 289*, 1751–1754.
7. Mulac-Jericevic, B., Lydon, J. P., DeMayo, F. J., and Conneely, O. M. (2003) Defective mammary gland morphogenesis in mice lacking the progesterone receptor B isoform. *Proc. Natl. Acad. Sci. U.S.A. 100*, 9744–9749.
8. Richer, J. K., Jacobsen, B. M., Manning, N. G., Abel, M. G., Wolf, D. M., and Horwitz, K. B. (2002) Differential gene regulation by the two progesterone receptor isoforms in human breast cancer cells. *J. Biol. Chem. 277*, 5209–5218.
9. Hopp, T. A., Weiss, H. L., Hilsenbeck, S. G., Cui, Y., Alfred, D. C., Horwitz, K. B., and Fuqua, S. A. (2004) Breast cancer patients with progesterone receptor PR-A-rich tumors have poorer disease-free survival rates. *Clin. Cancer Res. 15*, 2751–2760.
10. Connaghan-Jones, K. D., Heneghan, A. F., Miura, M. T., and Bain, D. L. (2007) Thermodynamic analysis of progesterone receptor-promoter interactions reveals a molecular model for isoform-specific function. *Proc. Natl. Acad. Sci. U.S.A. 104*, 2187–2192.
11. Connaghan-Jones, K. D., Heneghan, A. F., Miura, M. T., and Bain, D. L. (2008) Thermodynamic dissection of progesterone receptor interactions at the mouse mammary tumor virus promoter: Monomer binding and strong cooperativity dominate the assembly reaction. *J. Mol. Biol. 377*, 1144–1160.
12. Heneghan, A. F., Connaghan-Jones, K. D., Miura, M. T., and Bain, D. L. (2006) Cooperative DNA binding by the B-isoform of human progesterone receptor: Thermodynamic analysis reveals strongly favorable and unfavorable contributions to assembly. *Biochemistry 45*, 3285–3296.
13. Heneghan, A. F., Connaghan-Jones, K. D., Miura, M. T., and Bain, D. L. (2007) Coactivator assembly at the promoter: Efficient recruitment of SRC2 is coupled to cooperative DNA binding by the progesterone receptor. *Biochemistry 46*, 11023–11032.
14. Ptashne, M. (1988) How eukaryotic transcriptional activators work. *Nature 335*, 683–689.
15. Ackers, G. K., Johnson, A. D., and Shea, M. A. (1982) Quantitative model for gene regulation by lambda phage repressor. *Proc. Natl. Acad. Sci. U.S.A. 79*, 1129–1133.
16. Chahla, M., Wooll, J., Laue, T. M., Nguyen, N., and Senear, D. F. (2003) Role of protein-protein bridging interactions on cooperative assembly of DNA-bound CRP-CytR-CRP complex and regulation of the *Escherichia coli* CytR regulon. *Biochemistry 42*, 3812–3825.

17. Petri, V., Hsieh, M., Jamison, E., and Brenowitz, M. (1998) DNA sequence-specific recognition by the *Saccharomyces cerevisiae* "TATA" binding protein: Promoter-dependent differences in the thermodynamics and kinetics of binding. *Biochemistry 37*, 15842–15849.
18. Streaker, E. D., Gupta, A., and Beckett, D. (2002) The biotin repressor: Thermodynamic coupling of corepressor binding, protein assembly, and sequence-specific DNA binding. *Biochemistry 41*, 14263–14271.
19. Christensen, K., Estes, P. A., Onate, S. A., Beck, C. A., DeMarzo, A., Altmann, M., Lieberman, B. A., St. John, J., Nordeen, S. K., and Edwards, D. P. (1991) Characterization and functional properties of the A and B forms of human progesterone receptors synthesized in a baculovirus system. *Mol. Endocrinol. 5*, 1755–1770.
20. Connaghan-Jones, K. D., Heneghan, A. F., Miura, M. T., and Bain, D. L. (2006) Hydrodynamic analysis of the human progesterone receptor A-isoform reveals that self-association occurs in the micromolar range. *Biochemistry 45*, 12090–12099.
21. Heneghan, A. F., Berton, N., Miura, M. T., and Bain, D. L. (2005) Self-association energetics of an intact, full-length nuclear receptor: The B-isoform of human progesterone receptor dimerizes in the micromolar range. *Biochemistry 44*, 9528–9537.
22. Bain, D. L., Franden, M. A., McManaman, J. L., Takimoto, G. S., and Horwitz, K. B. (2000) The N-terminal region of the human progesterone A-receptor. Structural analysis and the influence of the DNA binding domain. *J. Biol. Chem. 275*, 7313–7320.
23. Bain, D. L., Franden, M. A., McManaman, J. L., Takimoto, G. S., and Horwitz, K. B. (2001) The N-terminal region of human progesterone B-receptors: Biophysical and biochemical comparison to A-receptors. *J. Biol. Chem. 276*, 23825–23831.
24. Philo, J. S. (2000) A method for directly fitting the time derivative of sedimentation velocity data and an alternative algorithm for calculating sedimentation coefficient distribution functions. *Anal. Biochem. 279*, 151–163.
25. Stafford, W. F. (1992) Boundary analysis in sedimentation transport experiments: A procedure for obtaining sedimentation coefficient distributions using the time derivative of the concentration profile. *Anal. Biochem. 203*, 295–301.
26. Van Holde, K. E. (1971) Physical Biochemistry, Prentice-Hall, Englewood Cliffs, CA.
27. Cohn, E. J., and Edsall, J. T. (1943) Proteins, Amino Acids and Peptides, Reinhold, New York.
28. Johnson, A. D., Poteete, A. R., Lauer, G., Sauer, R. T., Ackers, G. K., and Ptashne, M. (1981) Lambda repressor and cro—components of an efficient molecular switch. *Nature 294*, 217–223.
29. Laue, T. M., Shah, B. D., Ridgeway, T. M., and Pelletier, S. L. (1992) Analytical Ultracentrifugation in Biochemistry and Polymer Science, Royal Society of Chemistry, Cambridge.
30. Hamer, W. J., and Wu, Y.-C. (1972) Osmotic coefficients and mean activity coefficients of uni-univalent electrolytes in water at 25 °C. *J. Phys. Chem. Ref. Data 1*, 1047–1100.
31. Jantzen, H. M., Strahle, U., Gloss, B., Stewart, F., Schmid, W., Boshart, M., Miksicek, R., and Schutz, G. (1987) Cooperativity of glucocorticoid response elements located far upstream of the tyrosine aminotransferase gene. *Cell 49*, 29–38.
32. Brenowitz, M., Senear, D. F., Shea, M. A., and Ackers, G. K. (1986) Quantitative DNase footprint titration: A method for studying protein-DNA interactions. *Methods Enzymol. 130*, 132–181.
33. Brenowitz, M., Senear, D. F., Shea, M. A., and Ackers, G. K. (1986) Footprint titrations yield valid thermodynamic isotherms. *Proc. Natl. Acad. Sci. U.S.A. 83*, 8462–8466.
34. Hill, T. L. (1960) An Introduction to Statistical Thermodynamics, Dover Publications, New York.
35. Dang, Q. D., and Di Cera, E. (1996) Residue 225 determines the Na^+-induced allosteric regulation of catalytic activity in serine proteases. *Proc. Natl. Acad. Sci. U.S.A. 93*, 10653–10656.
36. Tsai, S. Y., Tsai, M.-J., and O'malley, B. W. (1989) Cooperative binding of steroid hormone receptors contributes to transcriptional synergism at target enhancer elements. *Cell 57*, 443–448.
37. Nayal, M., and Di Cera, E. (1996) Valence screening of water in protein crystals reveals potential Na^+ binding sites. *J. Mol. Biol. 256*, 228–234.
38. Gullans, S. R., Avison, M. J., Ogino, T., Giebisch, G., and Shulman, R. G. (1985) NMR measurements of intracellular sodium in the rabbit proximal tubule. *Am. J. Physiol. Renal Physiol. 249*, F160–F168.
39. László, B., Teréz, M., Miklós, E., Zoltán, K., and Lajos, T. (1997) Flow cytometric determination of intracellular free potassium concentration. *Cytometry 28*, 42–49.
40. Derfoul, A., Robertson, N. M., Lingrel, J. B., Hall, D. J., and Litwack, G. (1998) Regulation of the human Na/K-ATPase beta 1 gene promoter by mineralocorticoid and glucocorticoid receptors. *J. Biol. Chem. 273*, 20702–20711.
41. Boardman, L., Huett, M., Lamb, J. F., Newton, J. P., and Polson, J. M. (1974) Evidence for the genetic control of the sodium pump density in HeLa cells. *J. Physiol. 241*, 771–794.
42. Bowen, J. W., and McDonough, A. (1987) Pretranslational regulation of Na-K-ATPase in cultured canine kidney cells by low K^+. *Am. J. Physiol. Cell Physiol. 252*, C179–189.
43. Pressley, T. A. (1988) Ion concentration-dependent regulation of Na, K-pump abundance. *J. Membr. Biol. 105*, 187–195.
44. Pressley, T. A. (1992) Ionic regulation of Na^+,K^+-ATPase expression. *Semin. Nephrol. 12*, 67.
45. Pressley, T. A., Ismail-Beigi, F., Gick, G. G., and Edelman, I. S. (1988) Increased abundance of Na^+-K^+-ATPase mRNAs in response to low external K^+. *Am. J. Physiol. Cell Physiol. 255*, C252–C260.